ACS OMEGA

Open Access

http://pubs.acs.org/journal/acsodf

Article

Synthesis of Poly(ethylene terephthalate) Reinforced with Zinc Oxide Nanoparticles via Solution Blending for Prosthetic Socket Material: Physicochemical and Antibacterial Studies

Nur Aina Syafiqah Suhaimi, Nasrul Anuar Abd Razak,* Farina Muhamad, and Assayidatul Laila Nor Hairin

Cite This: *ACS Omega* 2026, 11, 36528−36538

Read Online

ACCESS | Metrics & More | Article Recommendations

ABSTRACT: This work synthesized recycled poly(ethylene terephthalate) (PET) with zinc oxide nanoparticles (1.0, 3.0, 5.0, and 7.0 wt %) via solution blending, aimed at transforming postconsumer plastic waste into high-value antibacterial materials for prosthetic socket applications. The PET/ZnO composites demonstrated homogeneous dispersion, improved mechanical hardness, and effective antibacterial activity, particularly at 7.0 wt % ZnO. Enhanced surface hydrophilicity and acceptable roughness were also observed. This approach improves prosthetic performance and promotes sustainable healthcare materials by utilizing plastic waste.

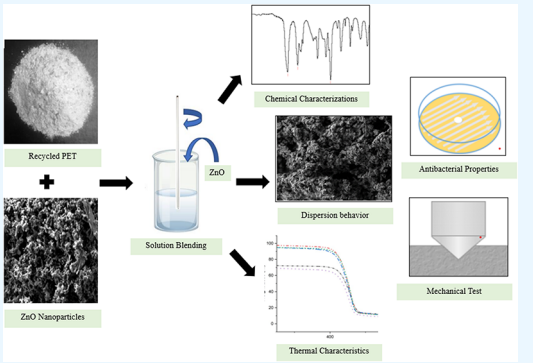

1. INTRODUCTION

Lower limb prosthetic sockets are essential biomedical interfaces that must balance load transmission, comfort, hygiene, and skin compatibility.[1] Conventional socket materials often face challenges such as moisture accumulation, bacterial colonization, and limited long-term comfort, leading to skin irritation or infection in a significant proportion of users.[2,3] These issues highlight the need for materials that are structurally robust, antibacterial, and comfortable for prolonged skin contact.

Poly(ethylene terephthalate) (PET) is a widely available thermoplastic known for its excellent mechanical strength, thermal stability, chemical resistance, and processability.[4,5] Despite these advantages, its biomedical applications, particularly in prosthetic interfaces, are limited due to surface hydrophobicity and lack of inherent bioactivity.[6] Upcycling postconsumer PET bottles into functional materials addresses environmental concerns while providing a sustainable source for advanced prosthetic interfaces.[7] Its processability also allows incorporation of functional nanofillers, such as ZnO nanoparticles, to enhance mechanical properties, surface wettability, and antibacterial activity.

To contextualize this work within prior PET/ZnO research, Table 1 summarizes representative studies, including their synthesis routes, ZnO loadings, processing methods, morphological observations, and targeted applications. Most previous studies employed relatively low ZnO concentrations due to common issues with agglomeration, and none have explored PET/ZnO systems for prosthetic sockets. Although surface modification of ZnO nanoparticles is sometimes used to mitigate agglomeration, this approach introduces additional chemical steps, increases fabrication cost, and may alter the antibacterial behavior of ZnO, making them less desirable for cost-effective, biocompatible prosthetic applications. Accordingly, the present study aims to synthesize PET/ZnO composites with higher ZnO loadings for prosthetic socket applications, employing a solution-blending mechanism designed to promote uniform nanoparticle dispersion at relatively low processing temperatures. This approach minimizes thermal degradation and reduces the likelihood of nanoparticle agglomeration, both of which are critical factors in achieving reliable mechanical and antibacterial performance.

Solution blending was selected in this study to achieve uniform dispersion of ZnO nanoparticles within the PET matrix, which is critical for maintaining consistent mechanical and surface properties. Compared with melt compounding or in situ polymerization, solution blending operates at lower

Received: September 18, 2025
Revised: January 7, 2026
Accepted: January 15, 2026
Published: June 17, 2026

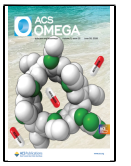

Table 1. Comparative Summary of PET/ZnO Nanocomposite Studies

ZnO Loadings (wt %)	synthesis route	processing method	key findings	applications	refs
1 wt %	ZnO incorporated into PET	Melt extrusion + injection molding	Low loading gives uniform distribution; improves crystallinity; no high-loading dispersion analysis.	Chemical/UV-resistant PET components	8
≤2 wt %	PET fibers functionalized with ZnO	Electrospinning	Homogeneous surface functionalization; no bulk matrix; good antibacterial properties.	Antibacterial textiles/wound dressings	9
1, 3, 5 wt %	Surface modification with citric acid	Ultrasonic-assisted solution mixing	Improved dispersion with surface-modified ZnO nanoparticles; Surface-treated ZnO improves dispersion at higher concentrations.	Packaging	10
1, 2, 3 wt %	ZnO/TiO_2 incorporated into PET	Extrusion	Nanoparticle agglomerations were observed, and the work primarily focused on UV stability rather than mechanical optimization.	UV-protection bottles	11
≤4 wt %	Solution Dispersion	Bilayer film casting	The surface became irregular with increasing ZnO content and reduced dispersion at higher loadings (3–4 wt %).	Antibacterial packaging	12

temperatures, thereby minimizing thermal degradation of PET and preserving its inherent mechanical integrity.[13,14] Improved nanoparticle distribution reduces the formation of large agglomerates that act as stress concentrators,[15,16] enabling better surface uniformity, hardness, and potential antibacterial functionality, which are key requirements for prosthetic socket applications.

Reinforcing PET with ZnO nanoparticles can improve both mechanical performance and antibacterial functionality. Hydroxyl groups on ZnO surfaces interact with PET ester linkages, enhancing interfacial adhesion and efficient stress transfer under load, while ZnO nanoparticles act as nucleation sites, potentially modifying PET crystallinity.[17] Antibacterial activity arises from reactive oxygen species (ROS) generation and Zn^{2+} ion release,[9] potentially reducing bacterial adhesion on prosthetic surfaces. Achieving these dual benefits depends critically on nanoparticle dispersion; previous studies have shown that poor dispersion or excessive agglomeration can negate both mechanical and antibacterial properties.[9,15] Therefore, solution blending in this work is intended to enable fine, uniform dispersion of ZnO nanoparticles, even at higher loadings, while maintaining the structural integrity required for prosthetic applications.

To comprehensively evaluate the suitability of the PET/ZnO nanocomposites for prosthetic socket use, multiple characterization techniques were employed: FTIR to assess chemical interactions; XRD for crystallinity and structural changes; DSC for thermal transitions; FESEM for morphological analysis and nanoparticle distribution; contact angle and surface roughness tests for evaluating wettability and skin-contact behavior; hardness testing to evaluate mechanical performance; and antibacterial assays to assess the efficacy of ZnO incorporation in reducing bacterial adhesion. Together, these analyses provide a complete assessment of the physicochemical properties relevant to both mechanical integrity and biological interface performance.

2. MATERIALS AND METHODS

2.1. Materials

The postconsumer PET bottles were collected, washed, and cut into smaller pieces of 1 cm × 1 cm. ZnO nanopowder (*Sigma-Aldrich, Malaysia*) with an average particle size of 100 nm was used as the filler material. Trifluoroacetic acid (CF_3COOH, analytical reagent) and dichloromethane (CH_2Cl_2, analytical reagent) purchased from *Sigma-Aldrich,Malaysia* were used as the solvents for solution blending of PET and ZnO nanoparticles.

2.2. Preparation of Recycled PET Powder

The PET pellets were dried in a vacuum oven for 24 h at 70 °C to expel excessive moisture within the materials, which can cause hydrolytic degradation under high temperatures. A 50 mL mixture of CF_3COOH and CH_2Cl_2 was prepared with a 1:5 ratio. 6 g of PET was put into the mixture of CF_3COOH and CH_2Cl_2 in a conical flask, which was heated in a water bath at 40 °C on a hot plate stirrer until the PET pellets were dissolved completely. 50 mL of ethanol was used to precipitate the recycled products in the solution. The precipitated powders were filtered out and dried in a vacuum oven for 24 h to remove excess moisture content.

2.3. Synthesis of PET/ZnO Composite Powder

Previously prepared recycled PET solution was placed in a 500 mL conical flask. ZnO nanoparticles were then put into the prepared solution with various concentrations (1.0, 3.0, 5.0, and 7.0 wt %). The mixture was stirred vigorously under a magnetic stirrer for 1 h. The final product of PET/ZnO composites was eluted with a nonsolvent, ethanol by precipitation technique with a ratio of 1:1 to the volume of

https://doi.org/10.1021/acsomega.5c09735
ACS Omega 2026, 11, 36528−36538

solvent. The precipitated final product was dried in a vacuum oven for 24 h at 70 °C.

2.4. Characterization of PET/ZnO Composite Powders

The interaction of ZnO in the PET matrix was observed through FTIR analysis (PerkinElmer Spectrum 400 FTIR spectrometer, USA). The crystalline phase of the synthesized PET/ZnO was characterized by XRD analysis with a Miniflex 600C X-ray diffractometer (Rigaku, Japan). The effects of incorporating ZnO nanoparticles on the thermal stability were analyzed using a TGA 4000 (PerkinElmer, USA) with a 20.0 °C/min heating rate, from room temperature to 500 °C under a nitrogen atmosphere; while the thermal behavior of PET, such as the glass transition temperature,[18] melting temperature (T_m), and crystallization temperature (T_c), were studied by DSC using a TA Instruments DSC Q20 (TA Instruments, USA). DSC also evaluated the crystallization behavior of the composites. The heating rate was 10.0 °C/min from room temperature to 290 °C; then, cooling was performed at the same rate under the protection of a nitrogen atmosphere. The degree of crystallinity, X_c, of the samples, measured by DSC, is then calculated using the following equation.

$$X_c = \frac{\Delta H_m - \Delta H_{cc}}{\Delta H_m^\circ} \cdot 100\% \quad (1)$$

In this equation, ΔH_m is the heat of melting, ΔH_{cc} is the cold crystallization enthalpy, and ΔH_m° is the heat of melting of a pure crystalline sample, which is 140 J/g according to the literature.[19]

The morphological properties of PET/ZnO composite powders with different concentrations of ZnO during solution blending were evaluated by FESEM (Zeiss Sigma) on gold-coated powders. The composites in powder form were then compacted and sintered using the powder compaction technique for property evaluation.

2.5. Water Contact Angle

The hydrophilicity of the surface of the PET/ZnO composite samples was assessed by Attension Theta (Sweden) equipped with image-capturing software. The wetting angle at which the liquid formed on the sample's surface was determined using the sessile drop method. A water droplet was placed on the surface of the samples and the contact angle was recorded after 10 s. Three measurements were taken for mean and standard deviation calculations.

2.6. Surface Roughness

The PET/ZnO composite samples were evaluated for their respective surface roughness using a tabletop contact profilometer device (Mitutoyo SurfTest). The direction of the surface profile measurements was ensured to be perpendicular to the direction of the tool. A total of 5 trials were carried out to represent each surface. Three different R-values, which are also the common roughness parameters, R_a (arithmetic average roughness), R_q (root-mean-square roughness), and R_z (average ten-point of the profile), were measured. The 5 sets of profiles were then used to provide the standard deviation and mean calculations.

2.7. Antibacterial Activity

Escherichia coli and *Staphylococcus aureus* are prominent bacteria commonly found on human skin, causing severe skin infections. This study used the standard isolate *E. coli* ATC 25922 and *S. aureus* ATC 25923 as the bacteria to test the antibacterial properties of the synthesized PET/ZnO composites. Bacterial strains were placed on agar plates and incubated for 24 h under aerobic conditions at 37 °C. The colony suspension was prepared by selecting 10−20 isolated colonies in 5 mL saline solution (0.85% NaCl). The bacterium was then swabbed over the entire surface of the agar 3 times, each time at an angle of 60°. The sample containing the extracts was then transferred to a test plate and assayed on a triplicate agar medium plate. After incubation at 37 °C for 24 h, the zone of inhibition was measured. The test was repeated 3 times for each sample for mean and standard deviation calculations.

2.8. Hardness Test

The hardness test was conducted on the neat PET and PET/ZnO composites using a Vickers hardness tester (Mitutoyo Corp, Japan) with the diamond pyramid indenter. The samples were tested according to the international standard ASTM D 2240 applied to an HV0.2 load with a holding time of 10 s. Then, the width of the indentation on the samples was observed and measured using an optical microscope with 10× magnification and calculated according to the hardness (HV) equation as indicated below in eq 2.

$$\mathrm{HV} = 1.8544\frac{P}{d^2} \quad (2)$$

In this equation, P is the indentation load (kgf) while d is the mean diameter of the diamond-shaped indent. The hardness test was performed 4 times for each sample at 4 sites for mean and standard deviation calculations.

2.9. Statistical Analysis

All results are presented as mean ± the standard deviation.[20] The one-way ANOVA (SPSS Version 29) was performed to compare group differences, followed by a posthoc Tukey test, with $p < 0.05$ considered statistically significant.

3. RESULTS AND DISCUSSION

3.1. Synthesis of PET/ZnO Composites

3.1.1. Fourier-Transform Infrared Spectroscopy (FTIR). Figure 1 exhibits the FTIR spectra of neat PET and

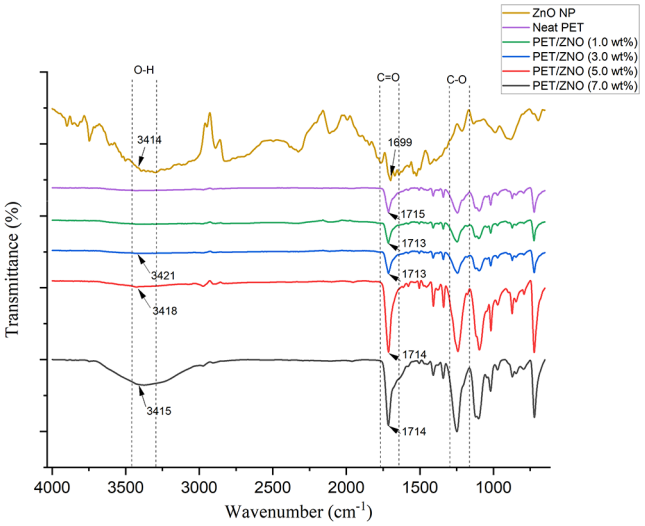

Figure 1. FTIR spectra of ZnO, Neat PET, and PET-ZnO Composites.

the PET/ZnO composite incorporated through solution blending. Recycled PET exhibited several characteristic absorption peaks at 1240 and 1714 cm^{-1}, corresponding to the aromatic esters and −C═O. Other peaks such as 1340 cm^{-1} (stretching of C−O group), 1504 cm^{-1} (vibrations aromatic skeleton with stretching of C═C), 2970 cm^{-1} (stretching of C−H), 1096 and 1050 cm^{-1} (methylene group, and vibration of C−O bond of ester), and 972, 872, and 848 cm^{-1} (aromatic rings) were also present in the FTIR spectra in Figure 1. These similar peaks were observed in the previous literature, corresponding to the typical PET peaks.[21,22] A significant absorption peak in the PET/ZnO composites spectrum (~3415 cm^{-1}) was observed, confirming the formation of intermolecular hydrogen bonds between the O−H group of the PET and the surface of ZnO, indicating

https://doi.org/10.1021/acsomega.5c09735
ACS Omega 2026, 11, 36528−36538

good filler−matrix interaction.[23] This demonstrated the successful compounding of ZnO nanoparticles in the PET samples.

3.2. Thermal Characteristics of PET/ZnO Composites

3.2.1. Differential Scanning Calorimetry (DSC). The DSC thermograms of the neat PET and PET/ZnO composites are shown in Figure 2, and the thermal properties of the

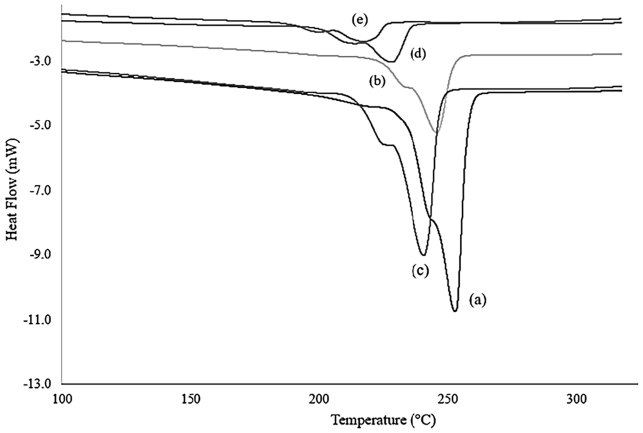

Figure 2. 2nd heating of DSC thermograms of (a) neat PET and PET with the addition of (b) 1.0, (c) 3.0, (d) 5.0, and (e) 7.0 wt % of ZnO nanoparticles.

Table 2. Thermal Properties of PET/ZnO Composites Obtained from DSC Data from the 1st Heating

sample	T_{cc} (°C)	T_m (°C)	ΔH_{cc} (J/g)	ΔH_m (J/g)	X_c (%)
Neat PET	215.4	252.8	523.3	469.1	38.7
PET/ZnO (1 wt %)	202.3	246.0	1092	1060	22.9
PET/ZnO (3 wt %)	199.7	241.2	207.7	161.8	32.8
PET/ZnO (5 wt %)	189.1	229.2	642.2	721.5	56.6
PET/ZnO (7 wt %)	178.4	218.5	231.7	307.9	54.4

samples related to each pattern are listed in Table 2. The composite systems had the T_m shifted to lower temperatures by incorporating ZnO. The decrease in T_m was also observed in several other studies with PET/ZnO composites.[24,25] The progressive reduction in T_m from 252.8 to 218.5 °C as ZnO content increases can be attributed to the constrained mobility of PET chains at the ZnO interface, which hinders the formation of perfect crystalline regions. This leads to the development of less stable, imperfect crystallites that require less thermal energy to melt, consistent with prior observations in polymer nanocomposites.[26] It can also be observed that the crystallization in all PET/ZnO composites was improved, as indicated in Table 2. The presence of ZnO nanoparticles lowers the energy barrier for nucleation due to their high surface area and interfacial interaction with the PET matrix. According to nucleation theory, heterogeneous nucleation sites reduce the critical free energy for crystal formation. The observed decrease in T_{cc} and increase in X_c for 5.0 and 7.0 wt % samples suggest that ZnO acts as an effective heterogeneous nucleating agent, promoting more ordered crystalline regions.[27]

These results show that incorporating ZnO nanoparticles into the PET matrix can lead to constrained chain mobility due to interactions at the polymer−nanoparticle interface. This restriction in chain movement affects crystallization behavior, potentially resulting in the formation of imperfect or less-ordered crystalline regions. Such effects have been observed in studies examining the crystallization behavior of PET/ZnO nanocomposites, where alterations in crystallization temperature and degree of crystallinity were reported, indicating the influence of ZnO on chain dynamics and crystal formation[28,29]

The thermal data also showed an irregular trend in the degree of crystallinity, which occurred upon incorporating 1.0 and 3.0 wt % of ZnO nanoparticles. It may be speculated that the presence of polymeric or inorganic components formed during the process has hindered the effects of ZnO on the crystallization of PET.

Regarding thermal analysis, Table 3 indicates that the addition of ZnO causes a progressive decrease in T_{onset},

Table 3. Thermal Analysis Data of Neat PET and PET/ZnO Composites

sample	T_{onset} (°C)	T_{max} (°C)
Neat PET	428.45	458.86
PET/ZnO (1 wt %)	423.52	456.08
PET/ZnO (3 wt %)	405.22	459.22
PET/ZnO (5 wt %)	404.61	457.67
PET/ZnO (7 wt %)	401.98	459.28

indicating that ZnO promotes earlier chain scission and accelerates the formation of volatile degradation fragments at lower temperatures. The reduction of thermal stability might be attributed to the catalytic activity of ZnO on the polymer matrix.[30] However, T_{max} does not follow the same trend; instead, the 3.0 and 7.0 wt % composites show a slight increase in T_{max} relative to neat PET. The increase in T_{max} at 3.0 wt % corresponds to the best nanoparticle dispersion; in contrast, the increase at 7.0 wt % is likely due to the formation of rigid ZnO microdomains that delay the maximum decomposition rate. This suggests a dual effect of ZnO: it promotes early PET degradation but also stabilizes intermediate products, slightly delaying the peak degradation rate. Overall, neat PET is more thermally stable at the onset, while ZnO addition lowers T_{onset} but slightly delays the peak degradation, indicating a modified but not inherently improved thermal stability in the composites.

3.3. Crystallization Behavior of PET/ZnO Composites

3.3.1. X-ray Diffraction (XRD). X-ray diffraction (XRD) analysis was performed to investigate the crystalline structure of the PET/ZnO nanocomposites. The XRD patterns of neat PET and PET/ZnO composites with varying ZnO contents (1.0, 3.0, 5.0, and 7.0 wt %) are shown in Figure 3.

Neat PET exhibited characteristic semicrystalline diffraction peaks at $2\theta \approx 16.9$, 23.1, 25.0, and 26.2°, which correspond to the (010), (100), and overlapping (110) crystalline planes. These results are consistent with typical PET crystal structures reported in the literature.[8,10] The presence of these peaks confirms that the recycling and blending process preserved the structural integrity of PET.

Upon incorporation of ZnO nanoparticles, additional peaks appeared at $2\theta \approx 31.8$ and 47.2°, corresponding to the (100) and (102) planes of the hexagonal wurtzite phase of ZnO (JCPDS Card No. 36−1451).[31] The intensity of these ZnO-related peaks increased progressively with ZnO content, particularly in the 5.0 and 7.0 wt % composites, indicating a

https://doi.org/10.1021/acsomega.5c09735
ACS Omega 2026, 11, 36528−36538

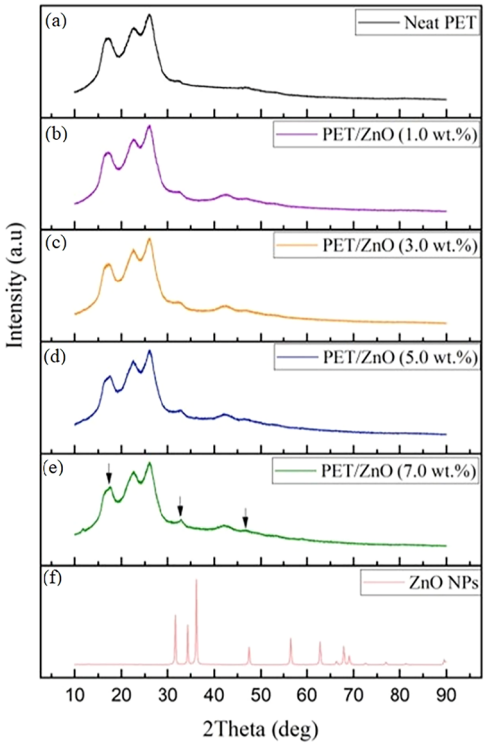

Figure 3. XRD patterns of (a) neat PET, PET/ZnO composites containing (b) 1 wt %, (c) 3 wt %, (d) 5 wt %, and (e) 7 wt % of ZnO nanoparticles, and (f) ZnO nanoparticles. ZnO peaks corresponding to (100) and (102) planes are evident at ∼31.8° and ∼47.2°, respectively, confirming the presence of hexagonal ZnO (JCPDS 36−1451).

greater degree of ZnO crystallinity and successful dispersion in the PET matrix. This may be due to the ZnO nanoparticles acting as nucleating agents, intermolecular attractions, and polymer chain mobility.[10]

Notably, the peak around 36.2°, corresponding to the (101) reflection of ZnO, was weak in some spectra. This may be due to the orientation of ZnO crystallites, relatively low concentration, or overlapping with the amorphous background of PET. Slight shifts in XRD peak positions were observed, likely due to interfacial strain between the PET matrix and ZnO nanoparticles. These shifts can be attributed to lattice distortions arising from nanoparticle−polymer interactions.[10]

Overall, the XRD results confirm that ZnO nanoparticles were successfully incorporated into the PET matrix without significantly disrupting the PET's crystalline structure. The emergence of distinct ZnO peaks, alongside preserved PET crystallinity, supports the composite's structural compatibility and aligns well with the increased crystallinity observed in the DSC analysis.

3.4. Morphological Analysis of PET/ZnO Composites

3.4.1. Field-Emission Scanning Electron Microscopy (FESEM). The FESEM micrographs (Figure 4) reveal distinct surface characteristics that evolve with increasing ZnO concentration. At low ZnO loadings (1.0−3.0 wt %), the nanoparticles appear finely and uniformly distributed within the PET matrix, indicating strong interfacial compatibility and homogeneous dispersion of filler particles via solution blending. This uniformity reduces phase separation and supports the observed mechanical improvements.

At higher ZnO concentrations (5.0−7.0 wt %), the FESEM images show clear signs of localized nanoparticle clustering, particularly within the etched surface features (Figure 4e,f). Although solution blending provides a more favorable initial dispersion than low-shear melt or dry compounding, it cannot fully avoid agglomeration at elevated loadings. As the system approaches a percolation-like threshold, particle−particle interactions increasingly dominate over particle−polymer interactions, leading to the formation of microclusters. Importantly, the resulting aggregates represent limitations in polymer-inorganic nanocomposites fabrication rather than matrix−filler phase failure.[32,33] Consistent with reports where conventional compounding routes often cause mechanical deterioration beyond 3−4 wt % due to severe agglomeration and weak interfacial adhesion, the PET/ZnO composites in this study still demonstrate improved hardness and antibacterial activity up to 7 wt %. This is attributed to the preserved interfacial integrity and the ability of ZnO microdomains to act as rigid reinforcing phases, which continue to contribute positively to load transfer despite their localized clustering.[34]

Furthermore, the absence of large voids or polymer−filler phase gaps at all loadings suggests a strong filler−matrix interfacial adhesion, possibly enhanced by hydrogen bonding between ZnO hydroxyl groups and ester/carboxyl functionalities in PET.[26,35] This is critical in maintaining load transfer efficiency and avoiding stress concentration sites under mechanical strain.

3.5. Hydrophilicity Behavior of PET/ZnO Composites

Generally, bacterial adhesion greatly depends on the wettability of the interaction surfaces. Surface hydrophobicity is among the factors that affect bacterial adhesion and has a lower resistance to bacterial adhesion[36,37]

PET matrices with ZnO nanoparticles at different concentrations were tested for contact angle measurement, as depicted in the chart in Figure 5. Upon incorporating the ZnO nanofiller, the contact angle is getting smaller as ZnO has high hydrophilic properties.[25] This enhancement is primarily attributed to surface hydroxyl (−OH) groups on ZnO nanoparticles, which are known to form hydrogen bonds with water molecules, facilitating greater water affinity.[38] The observed wettability behavior might also be influenced by the surface morphology induced by nanoparticle incorporation. According to the Wenzel model, surface roughness amplifies the intrinsic wettability of a material.[39] Since ZnO is hydrophilic, increased nanoscale roughness arising from well-dispersed nanoparticles at 3.0 wt % further decreased the contact angle, indicating improved hydrophilicity. This interpretation is consistent with the pronounced hydrophilic behavior observed at the optimal ZnO loading of 3.0 wt %, where increased hydroxyl functionality and nanoscale texturing contributed to superior wettability.

However, further increases in ZnO loadings (5.0 and 7.0 wt %) reversed this trend, producing higher contact angles indicative of reduced hydrophilicity. This can be attributed to nanoparticle agglomeration at higher loadings, which disrupts surface uniformity, as confirmed by the FESEM micrographs.

Regardless, all measured water contact angles fell within the acceptable range for prosthetic socket materials (60°−130°), comparable to those of commercially used materials such as silicone, polyurethane, and closed-cell polyethylene foam.[40]

https://doi.org/10.1021/acsomega.5c09735
ACS Omega 2026, 11, 36528−36538

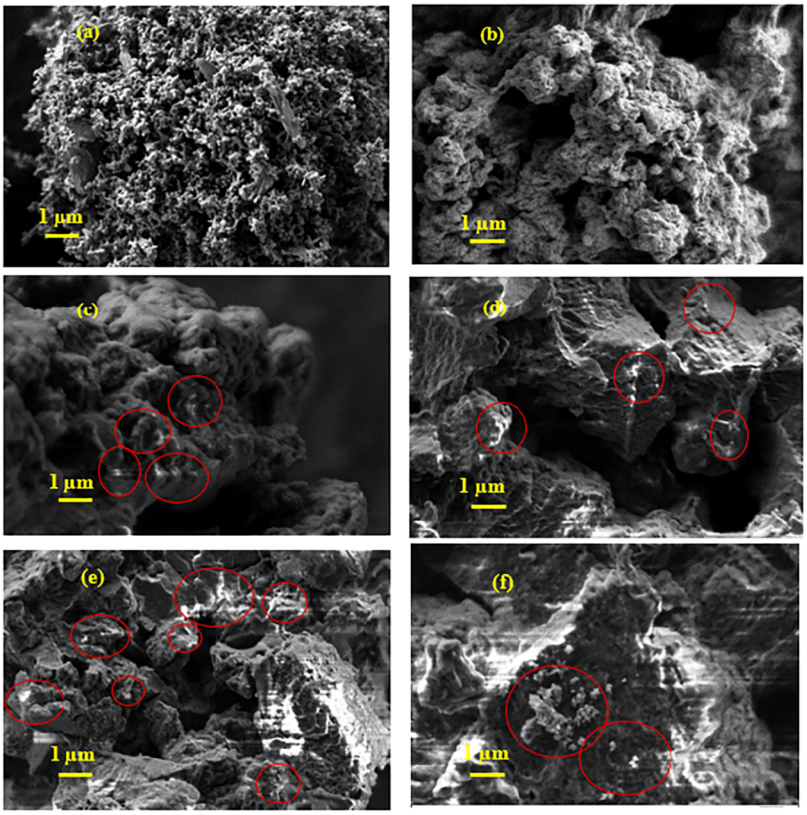

Figure 4. FESEM micrographs of (a) ZnO nanoparticles, (b) neat PET, and PET/ZnO composites at (c) 1.0 wt %, (d) 3.0 wt %, (e) 5.0 wt %, and (f) 7.0 wt % concentrations.

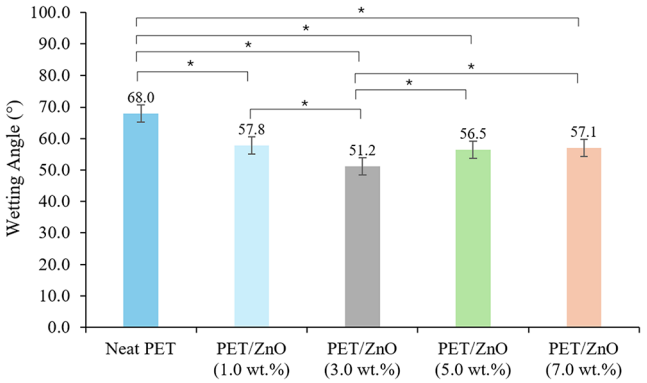

Figure 5. Contact angle for neat PET and PET with 1.0, 3.0, 5.0, and 7.0 wt % ZnO nanoparticles. Significantly different groups are represented by *($p < 0.05$).

These values indicate favorable surface wettability, supporting the suitability of composites for prolonged skin contact.

3.6. Surface Roughness of PET/ZnO Composites

The surface roughness (R_a, R_q, and R_z) of the composites at different ZnO concentrations is presented in Table 4 and illustrated in Figure 6. Based on Figure 6, surface roughness increased with increasing ZnO concentrations, with 7.0 wt % surface being the roughest (R_a = 3.08 ± 0.8 μm, R_q = 3.39 ± 1.09 μm, and R_z = 22.18 ± 1.45 μm) and the neat PET sample being the smoothest (R_a = 1.93 ± 0.4 μm, R_q = 2.12 ± 1.05 μm, and R_z = 13.9 ± 1.19 μm). This increase in surface roughness may have implications for bacterial adhesion, as rougher surfaces provide more surface area and microtopographical features that facilitate bacterial retention.[41]

Table 4. Surface Roughness Values of Neat PET and PET/ZnO Composites at Various Concentrations[a]

sample	average surface roughness (μm)		
	R_a	R_q	R_z
Neat PET	1.93 ± 0.4[a]	2.12 ± 1.05[a]	13.90 ± 1.19[a]
PET/ZnO (1.0 wt %)	2.39 ± 0.9[ab]	2.63 ± 1.03[b]	17.21 ± 1.21[b]
PET/ZnO (3.0 wt %)	2.64 ± 0.6[b]	2.90 ± 1.03 [b]	19.01 ± 1.42[b]
PET/ZnO (5.0 wt %)	2.78 ± 0.6[bc]	3.06 ± 1.04[b]	20.02 ± 1.44[b]
PET/ZnO (7.0 wt %)	3.08 ± 0.8[c]	3.39 ± 1.09[c]	22.18 ± 1.45[c]

[a]Different superscript letters (a, b, c) within each column indicate statistically significant differences between groups at $p < 0.05$ (Tukey HSD).

The progressive increase in surface roughness with ZnO loading can be attributed to two main factors: (1) the onset of nanoparticle agglomeration and heterogeneity at higher loadings and (2) the increased surface topography introduced by agglomerated nanoparticles, causing irregular features.[42,43] This is particularly evident at 5.0 and 7.0 wt %, where mild clustering and surface defects were observed in FESEM images.

From a physicochemical perspective, surface roughness influences bacterial adhesion by providing microniches that protect bacterial colonies from shear stress and allow anchoring via van der Waals and electrostatic forces.[40,44] Although higher roughness (R_z = 22.18 μm for 7.0 wt %) could potentially favor bacterial anchoring, the simultaneous enhancement in surface hydrophilicity and the antibacterial properties of ZnO likely counterbalance this effect, limiting viable bacterial adhesion and colonization.

https://doi.org/10.1021/acsomega.5c09735
ACS Omega 2026, 11, 36528−36538

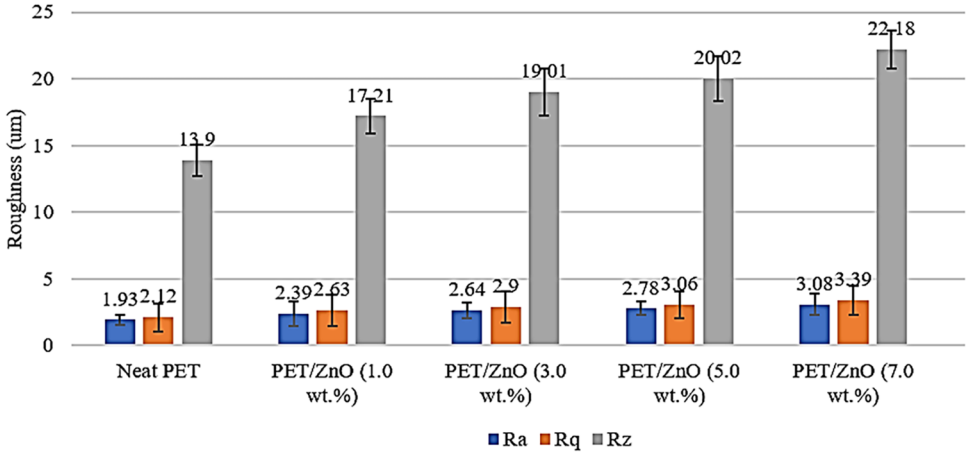

Figure 6. Surface roughness analysis for neat PET, and PET with 1.0, 3.0, 5.0, and 7.0 wt % ZnO nanoparticles. The results presented are the mean value of 5 measurements.

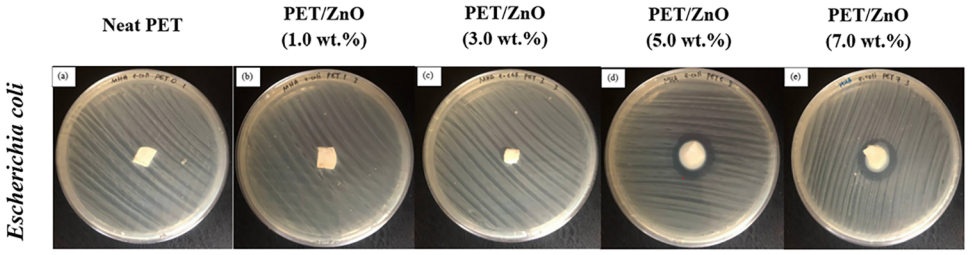

Figure 7. Antibacterial activities of (a) neat PET, and PET with (b) 1.0 wt %, (c) 3.0 wt %, (d) 5.0 wt %, and (e) 7.0 wt % ZnO nanoparticles against *E. coli* bacteria.

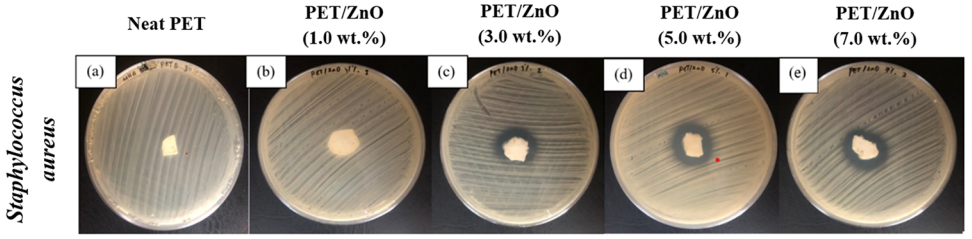

Figure 8. Antibacterial activities of (a) neat PET, and PET with (b) 1.0 wt %, (c) 3.0 wt %, (d) 5.0 wt %, and (e) 7.0 wt % ZnO nanoparticles against *S. aureus* bacteria.

Importantly, the measured roughness values remain within the acceptable thresholds for prosthetic socket interfaces, where moderate roughness can aid in mechanical interlocking with inner liners while avoiding excessive skin irritation.[45]

3.7. Antibacterial Activity of PET/ZnO Composites

Antibacterial properties are defined as the ability of the material to inhibit the growth of microorganisms, causing the bacteria to stop reproducing. Antibacterial agents can kill bacteria, making them fully safe on living tissues or human skin.[46] Commercialized materials for on-skin applications like prostheses typically do not exhibit significant inhibition zones against bacteria, as the products are not intended to have antibacterial features. Hence, this study determined the antibacterial activity of PET/ZnO composites against the *S. aureus* (Gram-positive) and *E. coli* (Gram-negative) bacteria, usually found on human skin, using qualitative measurement (inhibition zone method).

Figures 7 and 8 illustrate the inhibition zones of PET/ZnO nanocomposites against *E. coli* and *S. aureus*, respectively, while the corresponding quantitative measurements are summarized in Table 5. Neat PET (Figure 7a) and the composite containing 1.0 wt % ZnO (Figure 7b) showed no observable inhibition zones. measurable inhibition effect emerged at 3.0 wt % ZnO (1.73 ± 0.04 mm), with a significant increase at 5.0 and 7.0 wt % ZnO, recording inhibition zones of 23.07 ± 1.69 and 24.12 ± 2.38 mm, respectively. A similar trend was

Table 5. Inhibition Zone Diameter of PET/ZnO Composites against *E. coli* and *S. aureus* at 1.0, 3.0, 5.0, and 7.0 wt % ZnO Concentrations[a]

ZnO concentrations (wt %)	*E. coli* (mm)	*S. aureus* (mm)
0	0.00 ± 0.00^{d}	0.00 ± 0.00^{a}
1.0	0.00 ± 0.00^{d}	13.72 ± 1.05^{b}
3.0	1.73 ± 0.280^{c}	15.02 ± 1.81^{b}
5.0	23.07 ± 1.38^{a}	25.23 ± 0.08^{c}
7.0	24.12 ± 1.94^{a}	27.22 ± 0.37^{c}

[a]Different superscript letters (a, b, c) within each column indicate statistically significant differences between groups at $p < 0.05$ (Tukey HSD).

https://doi.org/10.1021/acsomega.5c09735
ACS Omega 2026, 11, 36528−36538

observed against *S. aureus* (Figure 8a). Neat PET exhibited no inhibition, while the composite with 1.0 wt % ZnO showed a notable antibacterial effect (13.72 ± 1.05 mm), which further increased to 15.02 ± 1.81, 25.23 ± 0.08, and 27.22 ± 0.37 mm at ZnO loadings of 3.0, 5.0, and 7.0 wt %, respectively.

Enhanced antibacterial activity can be attributed to multiple mechanisms associated with ZnO nanoparticles. One major factor is the release of Zn^{2+} ions in aqueous environments, which penetrate bacterial membranes and interact with protein thiol groups, leading to structural disruption and cell death.[47−49] Additionally, ZnO nanoparticles can interact directly with bacterial membranes, inducing leakage of intracellular components and compromising membrane integrity.[12,49] Another important mechanism involves the generation of reactive oxygen species (ROS), such as hydroxyl radicals ($^{\bullet}OH$), superoxide anions ($O_2^{\bullet-}$), and hydrogen peroxide (H_2O_2), even under ambient light due to ZnO's wide bandgap (~3.3 eV).[50] These ROS contribute to oxidative stress, lipid peroxidation, and DNA damage, ultimately leading to bacterial inactivation.[51]

While ZnO nanoparticles are often reported to be more effective against Gram-negative bacteria due to their thinner peptidoglycan layers and more permeable outer membranes, this study showed greater inhibition against *S. aureus* (Gram-positive). The influence of the polymer matrix on ZnO dispersion, surface exposure, and ion release kinetics may explain this reversal.[51] In solid-state systems like PET, the matrix properties modulate the interaction between ZnO nanoparticles and the bacterial cell wall. *S. aureus*, with its exposed peptidoglycan layer, may be more susceptible compared to *E. coli*, whose outer membrane, rich in lipopolysaccharides, can hinder Zn^{2+} diffusion and ROS penetration. Similar antibacterial behaviors have been reported in other polymer−ZnO nanocomposites.[9,24]

The results indicated that PET/ZnO composites can reduce the growth of microorganisms that cause bacterial infections and skin disorders in prosthetic users. Therefore, the synthesized composites inhibited the proliferation of bacteria in the presence of ZnO nanoparticles.

3.8. Hardness of PET/ZnO Composites

The Vickers hardness of the neat PET and PET/ZnO composites is depicted in Figure 9. A notable increase in hardness is observed with increasing ZnO content, rising from 15.75 ± 0.50 for neat PET to 23.69 ± 0.37 (Shore D hardness) for the 7.0 wt % ZnO composite. The increase in hardness reflects improved load transfer from the matrix to the ZnO particles, increasing mechanical performance.[52] ZnO has been frequently reported as an effective filler in improving mechanical performance.[8,53,54]

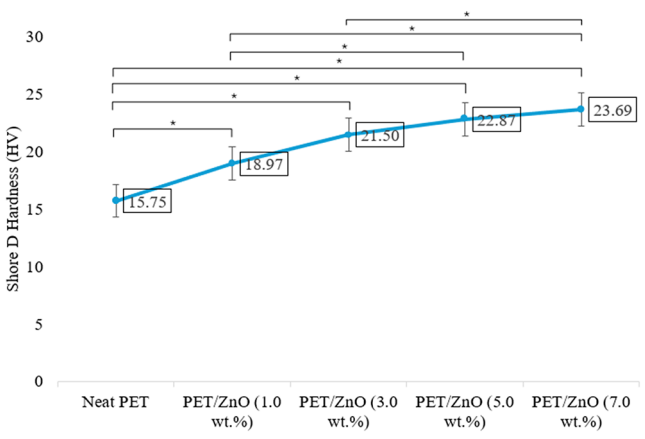

Figure 9. Vickers' hardness test (Shore D) of PET/ZnO Composites at different concentrations. Significantly different groups are represented by *($p < 0.05$).

According to the Halpin−Tsai model, mechanical reinforcement in particulate-filled polymers depends on filler volume fraction and aspect ratio. The nearly uniform dispersion observed up to 5.0 wt % creates efficient load-bearing pathways. At 7.0 wt %, despite minor aggregation, the percolation threshold may have been reached, enabling the development of a continuous filler network. This network likely enhances interfacial adhesion and limits plastic deformation of the matrix under applied stress.[55]

These results may also be due to the improved crystallization, corresponding to the DSC and XRD data. Generally, an increased degree of crystallinity will enhance the strength of the polymer, affecting the mechanical properties positively.[17] The ZnO nanoparticles may have also filled the voids and spaces present in the matrix. Therefore, more voids are filled in with increasing ZnO concentrations, increasing the hardness values and indentation resistance.[56] The reinforcing particles successfully strengthen the matrix, improving the resistance of the composite to applied pressures.

Commonly used thermoplastic materials like high-density polyethylene (HDPE) and polypropylene (PP) have a high hardness value typically between 60 and 80 on the Shore D scale.[57] However, the hardness value of some other prosthetic materials, such as silicone rubber and polyurethane, could be between 15 and 80 on the Shore A scale, which are considered soft materials.[58] Therefore, according to the durometer shore hardness scale, the value obtained by the PET/ZnO composites from this study was still within the acceptable range for prosthetic sockets, indicating the composites' suitability as a potential material.

3.9. Biocompatibility and Cytotoxicity Considerations

Although ZnO nanoparticles are widely recognized for their antibacterial properties, their incorporation into polymer matrices may also introduce biocompatibility concerns, particularly at higher concentrations. ZnO nanoparticles are known to exhibit dose-dependent biological responses, primarily governed by Zn^{2+} ion release, ROS generation, and direct membrane contact.[59,60] Studies on ZnO-reinforced polymeric systems, including PET- and polyester-based nanocomposites, have consistently shown that low ZnO concentrations (≤2−3 wt %%) typically retain cytocompatibility, supporting normal fibroblast and keratinocyte viability due to controlled ion diffusion and the physical barrier provided by the polymer matrix.

However, at higher ZnO concentrations, nanoparticle agglomeration becomes more pronounced, leading to localized regions of elevated Zn^{2+} release and ROS accumulation. These effects have been linked to oxidative stress, mitochondrial damage, or reduced cell proliferation in related polymer/ZnO composites.[60−62] Because the current study incorporates comparatively high concentrations (up to 7.0 wt %), similar risks may arise, particularly at the upper end of the concentration range, where FESEM already shows particle agglomeration.

Nonetheless, the PET matrix acts as a diffusion-limiting barrier, and the ZnO nanoparticles are predominantly

https://doi.org/10.1021/acsomega.5c09735
ACS Omega 2026, 11, 36528−36538

embedded within the PET matrix rather than exposed on the surface; hence, Zn^{2+} release and direct cellular contact are expected to remain limited. Studies on PMMA/ZnO and PLA/ZnO nanocomposites have demonstrated that when metal-oxide nanoparticles are well entrapped within the polymer bulk, Zn^{2+} release remains low and cytocompatibility is generally preserved.[63,64] Comparable PET-based composites containing metal-oxide nanoparticles have also shown acceptable skin-contact biocompatibility when surface exposure and ion migration are minimized.

Overall, PET/ZnO composites with 1.0−3.0 wt % ZnO is expected to remain within safe cytocompatibility limits, whereas 5.0−7.0 wt % ZnO may warrant further evaluation due to possible ROS-mediated effects. These considerations are important for prosthetic socket applications, where prolonged contact with residual-limb skin requires minimizing inflammatory or cytotoxic responses. Future biological testing will therefore focus on determining safe ZnO thresholds and verifying long-term compatibility.

4. CONCLUSIONS

This study successfully synthesized PET/ZnO nanocomposites via solution blending, incorporating ZnO nanoparticles up to 7.0 wt % with minimal agglomeration as supported by FESEM and thermal analyses. The composites exhibited key performance enhancements, including increased mechanical hardness, improved hydrophilicity, and notable antibacterial activity, arising from favorable physicochemical interactions between PET and ZnO, such as interfacial adhesion and the nucleating effect of ZnO nanoparticles. These material-level improvements are particularly relevant for skin-contact prosthetic applications, where hygiene, comfort, and mechanical stability are critical. The enhanced antibacterial behavior and stable structural response position PET/ZnO composites as promising candidates for future prosthetic socket components. Additionally, the successful upcycling of postconsumer PET into a functional biomedical composite underscores the material's sustainability potential by supporting circular economy pathways and reducing plastic waste. Future work should focus on evaluating cytotoxicity and biocompatibility in vitro to ensure safe prolonged skin contact, investigating the influence of ZnO nanoparticle size and shape on dispersion, mechanical performance, and antibacterial efficacy to further optimize the composites, and assessing long-term mechanical stability and wear resistance under simulated prosthetic loading conditions to confirm durability in real-life applications. These directions provide practical and targeted guidance for advancing PET/ZnO nanocomposites toward functional prosthetic socket applications.

AUTHOR INFORMATION

Corresponding Author

Nasrul Anuar Abd Razak − *Department of Biomedical Engineering, Faculty of Engineering, Universiti Malaya, 50603 Kuala Lumpur, Malaysia; Magister of Biomedical Engineering, Department of Physics, Faculty of Science and Technology, Airlangga University, 60115 Surabaya, Indonesia*; Email: nasrul.anuar@um.edu.my

Authors

Nur Aina Syafiqah Suhaimi − *Department of Biomedical Engineering, Faculty of Engineering, Universiti Malaya, 50603 Kuala Lumpur, Malaysia*; orcid.org/0000-0002-1737-0302

Farina Muhamad − *Department of Biomedical Engineering, Faculty of Engineering, Universiti Malaya, 50603 Kuala Lumpur, Malaysia*

Assayidatul Laila Nor Hairin − *Department of Manufacturing & Materials Engineering, Faculty of Engineering, International Islamic University Malaysia, 53100 Kuala Lumpur, Malaysia*

Complete contact information is available at: https://pubs.acs.org/10.1021/acsomega.5c09735

Funding

This work was supported by Universiti Malaya Living Labs@UMSDC (Grant No: LL2023ECO003).

Notes

The authors declare no competing financial interest.

ACKNOWLEDGMENTS

The authors thank the CPOE research team for their insightful suggestions.

REFERENCES

(1) Wang, X.; Tao, Y.; Pan, S.; Fang, X.; Lou, C.; Xu, Y.; Wu, J.; Sang, M.; Lu, L.; Gong, X.; et al. Biocompatible and breathable healthcare electronics with sensing performances and photothermal antibacterial effect for motion-detecting. *npj Flexible Electron.* **2022**, *6* (1), No. 95.

(2) Quintero-Quiroz, C.; Botero, L. E.; Zárate-Triviño, D.; Acevedo-Yepes, N.; Escobar, J. S.; Pérez, V. Z.; Cruz Riano, L. J. Synthesis and characterization of a silver nanoparticle-containing polymer composite with antimicrobial abilities for application in prosthetic and orthotic devices. *Biomater. Res.* **2020**, *24* (1), No. 13.

(3) Wang, X.; Liu, Y.; Cheng, H.; Ouyang, X. Surface Wettability for Skin-Interfaced Sensors and Devices. *Adv. Funct. Mater.* **2022**, *32* (27), No. 2200260, DOI: 10.1002/adfm.202200260.

(4) Suhaimi, N. A. S.; Muhamad, F.; Abd Razak, N. A.; Zeimaran, E. Recycling of polyethylene terephthalate wastes: A review of technologies, routes, and applications. *Polym. Eng. Sci.* **2022**, *62* (8), 2355−2375.

(5) Mehdi, M.; Mahar, F.; Qureshi, U.; Khatri, M.; Khatri, Z.; Ahmed, F.; Kim, I.-S. Preparation of colored r-PET nanofibers from waste bottles: physico-chemical studies. *Adv. Polym. Technol.* **2018**, *37*, 2820−2827.

(6) Szafran, K.; Jurak, M.; Mroczka, R.; Wiącek, A. E. Surface Properties of the Polyethylene Terephthalate (PET) Substrate Modified with the Phospholipid-Polypeptide-Antioxidant Films: Design of Functional Biocoatings. *Pharmaceutics* **2022**, *14* (12), No. 2815.

(7) Yang, T.; Yang, Z.; Zhang, Y.; Hu, C.; Xie, Z.; Sun, Z.; Pang, X.; Chen, X. Upcycling of PET Waste: From One Polymer to Another Polymer. *Polym. Chem.* **2026**, *17*, 7−20.

(8) de Sousa Barros, A. B.; Farias, R. F.; Siqueira, D. D.; Luna, C. B. B.; Araujo, E. M.; Rabello, M. S.; Wellen, R. M. R. The Effect of ZnO on the Failure of PET by Environmental Stress Cracking. *Materials* **2020**, *13* (12), No. 2844.

(9) Vázquez, K.; Vanegas, P.; Cruzat, C.; Novoa, N.; Arrue, R.; Vanegas, E. Antibacterial and Antifungal Properties of Electrospun Recycled PET Polymeric Fibers Functionalized with Zinc Oxide Nanoparticles. *Polymers* **2021**, *13* (21), No. 3763.

(10) Mallakpour, S.; Javadpour, M. The potential use of recycled PET bottle in nanocomposites manufacturing with modified ZnO nanoparticles capped with citric acid: preparation, thermal, and morphological characterization. *RSC Adv.* **2016**, *6* (18), 15039−15047.

(11) Khani, M.; Pordel, M.; Davoodnia, A.; TavasoliFarsheh, A. Investigation of the effect of using ZnO/TiO2 nano particles on properties of the polyethylene terephthalate preform and beverage bottles *Int. J. Ind. Chem.*, **2022** *13* 2.
(12) Nasiri, S. L.; Azizi, M. H.; Movahedi, F.; Rahimifard, N.; Tavakolipour, H. Potential perspectives of CMC-PET/ZnO bilayer nanocomposite films for food packaging applications: physical, mechanical and antimicrobial properties. *J. Food Meas. Charact.* **2021**, *15* (4), 3731−3740.
(13) Rasilainen, I.; Lahtela, V.; Kärki, T. A review of plastic waste nanocomposites: assessment of features and applications. *Discover Nano* **2024**, *19* (1), No. 112.
(14) Sharip, N. S.; Ariffin, H.; Yasim-Anuar, T. A. T.; Andou, Y.; Shirosaki, Y.; Jawaid, M.; Tahir, P. M.; Ibrahim, N. A. Melt- vs. Non-Melt Blending of Complexly Processable Ultra-High Molecular Weight Polyethylene/Cellulose Nanofiber Bionanocomposite. *Polymers* **2021**, *13* (3), No. 404.
(15) Zare, Y. Study of nanoparticles aggregation/agglomeration in polymer particulate nanocomposites by mechanical properties. *Composites, Part A* **2016**, *84*, 158−164.
(16) Bhatnagar, T.; Baxi, P.; Sharma, K.; Nijhawan, G.; Jugran, S.; Satyanarayana, K.; Sharma, L.; Alhadrawi, M. Unlocking the Strength of Nanocomposites: Mitigating the Impact of Nanoparticle Agglomeration on Tensile Performance. *E3S Web Conf.* **2024**, *588*, No. 01007.
(17) Agrawal, H.; Awasthi, K.; Saraswat, Y. K.; Saraswat, V. K. ZnO nanoparticles favours heterogeneous nucleation in PET−ZnO nanocomposites. *Philos. Mag.* **2015**, *95* (21), 2306−2322.
(18) Anžlovar, A.; Primožič, M.; Švab, I.; Leitgeb, M.; Knez, Ž.; Žagar, E. Polyolefin/ZnO Composites Prepared by Melt Processing. *Molecules* **2019**, *24* (13), No. 2432.
(19) Thomsen, T. B.; Hunt, C. J.; Meyer, A. S. Standardized method for controlled modification of poly (ethylene terephthalate) (PET) crystallinity for assaying PET degrading enzymes. *MethodsX* **2022**, *9*, No. 101815.
(20) Tasdemir, S. E. M. Zinc oxide (ZnO), magnesium hydroxide [Mg(OH)2] and calcium carbonate (CaCO3) filled HDPE polymer composites: Mechanical, thermal and morphological properties. *Marmara Univ. J. Sci.* **2012**, *24* (4), 93−104, DOI: 10.7240/mufbed.v24i4.319.
(21) Wang, M.; Zhang, M.; Pang, L.; Yang, C.; Zhang, Y.; Hu, J.; Wu, G. Fabrication of highly durable polysiloxane-zinc oxide (ZnO) coated polyethylene terephthalate (PET) fabric with improved ultraviolet resistance, hydrophobicity, and thermal resistance. *J. Colloid Interface Sci.* **2019**, *537*, 91−100.
(22) dos Santos Pereira, A. P.; da Silva, M. H. P.; Lima, É. P., Junior; dos Santos Paula, A.; Tommasini, F. J. Processing and Characterization of PET Composites Reinforced With Geopolymer Concrete Waste. *Mater. Res.* **2017**, *20* (suppl 2), 411−420.
(23) He, J.; Shao, W.; Zhang, L.; Deng, C.; Li, C. Crystallization behavior and UV-protection property of PET-ZnO nanocomposites prepared by in situ polymerization. *J. Appl. Polym. Sci.* **2009**, *114* (2), 1303−1311.
(24) Jin, J.; Fang, L. J.; Tang, L.; Ji, P.; Wang, C. S.; Wang, H. P. Preparation of Nano Cu-ZnO/PET Fiber for Antibacterial Application. *Mater. Sci. Forum* **2017**, *898*, 2272−2278.
(25) Gao, W.; Zhou, B.; Liu, Y.; Ma, X.; Liu, Y.; Wang, Z.; Zhu, Y. The influence of surface modification on the structure and properties of a zinc oxide-filled poly(ethylene terephthalate). *Polym. Int.* **2013**, *62* (3), 432−438.
(26) Zhang, J.; Wen, B.; Wang, F.; Ding, Y.; Zhang, S.; Yang, M. In situ synthesis of ZnO nanocrystal/PET hybrid nanofibers via electrospinning. *J. Polym. Sci., Part B: Polym. Phys.* **2011**, *49* (19), 1360−1368.
(27) Zhao, Z.; Yang, Q.; Xiang, Z.; Kong, M.; Tang, D.; Huang, Y.; Liao, X.; Niu, Y. Effect of in situ poly(ethylene terephthalate) (PET) microfibrils on the morphological structure and crystallization behavior of isotactic polypropylene (iPP) under an intensive shear rate. *Polym. Adv. Technol.* **2015**, *26* (10), 1275−1284.
(28) Ali Mohsin, M.; Ali, I.; Elleithy, R.; al-zahrani, S. Effect of Nano-SiO2 & ZnO on the crystallization behaviour of polyethylene terephthalate nanocomposite. *J. Polym. Mater.* **2012**, *29*, 89−100.
(29) Cyras, V. P.; D'Amico, D. A.; Manfredi, L. B. Crystallization Behavior of Polymer Nanocomposites. In *Crystallization in Multiphase Polymer Systems*; Thomas, S.; Arif P, M.; Gowd, E. B.; Kalarikkal, N., Eds.; Elsevier, 2018; Chapter 10, pp 269−311.
(30) Virovska, D.; Paneva, D.; Manolova, N.; Rashkov, I.; Karashanova, D. Electrospinning/electrospraying vs. electrospinning: A comparative study on the design of poly(l-lactide)/zinc oxide non-woven textile. *Appl. Surf. Sci.* **2014**, *311*, 842−850.
(31) Greeshma, K. P.; Muthulingam, S.; Thamizselvi, R.; Dhanya, B. S. Antimicrobial studies and characterization of ZnO nanoparticles by chemical method. *GSC Adv. Res. Rev.* **2021**, *8* (2), 071−077.
(32) Alshammari, B. A.; Wilkinson, A. N.; Almutairi, G. Electrical, Thermal, and Morphological Properties of Poly(ethylene terephthalate)-Graphite Nanoplatelets Nanocomposites. *Int. J. Polym. Sci.* **2017**, *2017* (1), No. 6758127.
(33) Fang, Q.; Lafdi, K. Effect of nanofiller morphology on the electrical conductivity of polymer nanocomposites. *Nano Express* **2021**, *2* (1), No. 010019.
(34) Demir, E. C.; Benkaddour, A.; Aldrich, D. R.; McDermott, M. T.; Kim, C. I.; Ayranci, C. A predictive model towards understanding the effect of reinforcement agglomeration on the stiffness of nanocomposites. *J. Compos Mater.* **2022**, *56* (10), 1591−1604.
(35) Grămadă Pintilie, A. M.; Stoica Oprea, A. E.; Niculescu, A. G.; Bîrcă, A. C.; Vasile, B.; Holban, A. M.; Mihaiescu, T.; Serban, A. I.; Ciceu, A.; Balta, C.; et al. Zinc Oxide-Loaded Recycled PET Nanofibers for Applications in Healthcare and Biomedical Devices. *Polymers* **2025**, *17* (1), No. 45, DOI: 10.3390/polym17010045.
(36) Salatin, S.; Lotfipour, F.; Jelvehgari, M. A brief overview on nano-sized materials used in the topical treatment of skin and soft tissue bacterial infections. *Expert Opin. Drug Delivery* **2019**, *16* (12), 1313−1331.
(37) Lee, J.-H.; Jo, J.-K.; Kim, D.-A.; Patel, K. D.; Kim, H.-W.; Lee, H.-H. Nano-graphene oxide incorporated into PMMA resin to prevent microbial adhesion. *Dent. Mater.* **2018**, *34* (4), e63−e72.
(38) Cheng, S. L.; Syu, J. H.; Liao, S. Y.; Lin, C. F.; Yeh, P. Y. Growth kinetics and wettability conversion of vertically-aligned ZnO nanowires synthesized by a hydrothermal method. *RSC Adv.* **2015**, *5* (83), 67752−67758.
(39) Pan, Z.; Cheng, F.; Zhao, B. Bio-Inspired Polymeric Structures with Special Wettability and Their Applications: An Overview. *Polymers* **2017**, *9* (12), No. 725.
(40) Abram, A.; Zore, A.; Lipovž, U.; Košak, A.; Gavras, M.; Boltežar, Ž.; Bohinc, K. Bacterial Adhesion on Prosthetic and Orthotic Material Surfaces. *Coatings* **2021**, *11* (12), No. 1469.
(41) Yuan, Y.; Hays, M. P.; Hardwidge, P. R.; Kim, J. Surface characteristics influencing bacterial adhesion to polymeric substrates. *RSC Adv.* **2017**, *7* (23), 14254−14261.
(42) Edachery, V.; Swamybabu, V.; Adarsh, D.; Kailas, S. V. Influence of surface roughness frequencies and roughness parameters on lubricant wettability transitions in micro-nano scale hierarchical surfaces. *Tribiol. Int.* **2022**, *165*, No. 107316.
(43) Pal, A.; Dey, T. K.; Singhal, A.; Bindal, R. C.; Tewari, P. K. Nano-ZnO impregnated inorganic−polymer hybrid thinfilm nanocomposite nanofiltration membranes: an investigation of variation in structure, morphology and transport properties. *RSC Adv.* **2015**, *5* (43), 34134−34151.
(44) Darmani, H. Todar's Online Textbook of Bacteriology. 2006.
(45) Hagen, C. M. H.; Hognestad, A.; Knudsen, O. Ø.; Sørby, K. The effect of surface roughness on corrosion resistance of machined and epoxy coated steel. *Prog. Org. Coat.* **2019**, *130*, 17−23.
(46) Nekouei, F.; Kargarzadeh, H.; Nekouei, S.; Tyagi, I.; Agarwal, S.; Kumar Gupta, V. Preparation of Nickel hydroxide nanoplates modified activated carbon for Malachite Green removal from solutions: Kinetic, thermodynamic, isotherm and antibacterial studies. *Process Saf. Environ. Prot.* **2016**, *102*, 85−97.

(47) Ashraf, M.; Campagne, C.; Perwuelz, A.; Champagne, P.; Leriche, A.; Courtois, C. Development of superhydrophilic and superhydrophobic polyester fabric by growing zinc oxide nanorods. *J. Colloid Interface Sci.* **2013**, *394*, 545−553.
(48) Lai, Y.; Guo, Y.; Xu, L.; Chang, X.; Zhang, X.; Xu, G.; Shi, J. Plasma Enhanced Fluorine-Free Superhydrophobic Polyester (PET) Fabric with Ultra-Robust Antibacterial and Antibacterial Adhesion Properties. *Coatings* **2021**, *11*, No. 15.
(49) Fiedot-Toboła, M.; Ciesielska, M.; Maliszewska, I.; Rac-Rumijowska, O.; Suchorska-Wozniak, P.; Teterycz, H.; Bryjak, M. Deposition of Zinc Oxide on Different Polymer Textiles and Their Antibacterial Properties. *Materials* **2018**, *11* (5), No. 707.
(50) Kumar, R.; Umar, A.; Kumar, G.; Nalwa, H. S. Antimicrobial properties of ZnO nanomaterials: A review. *Ceram. Int.* **2017**, *43* (5), 3940−3961.
(51) Sirelkhatim, A.; Mahmud, S.; Seeni, A.; Kaus, N. H. M.; Ann, L. C.; Bakhori, S. K. M.; Hasan, H.; Mohamad, D. Review on Zinc Oxide Nanoparticles: Antibacterial Activity and Toxicity Mechanism. *Nano-Micro Lett.* **2015**, *7* (3), 219−242.
(52) Kesler, D.; Ariyawansa, B. P.; Rathnayake, H. Mechanical Properties and Synergistic Interfacial Interactions of ZnO Nanorod-Reinforced Polyamide−Imide Composites. *Polymers* **2023**, *15* (6), No. 1522.
(53) Mallakpour, S.; Behranvand, V. Nanocomposites based on biosafe nano ZnO and different polymeric matrixes for antibacterial, optical, thermal and mechanical applications. *Eur. Polym. J.* **2016**, *84*, 377−403.
(54) Tao, J.; Wang, T.; Dong, X.; Xiaoqian, S. Mechanical properties and crystallization behaviors of nanostructured-Zno/PET in-situ composites. *J. Nanosci. Nanotechnol.* **2006**, *6* (12), 3939−3942.
(55) Zare, Y. Development of Halpin-Tsai model for polymer nanocomposites assuming interphase properties and nanofiller size. *Polym. Test.* **2016**, *51*, 69−73.
(56) H S, H. S.; N, K.; Naik, Y.; Kumar, R.; Prasad, A. Enhanced Wear Characteristics of UHMWPE Composite Reinforced with Nano ZnO: Experimental Investigation and Microstructural Analysis. *Tuijin Jishu/J. Propul. Technol.* **2023**, *44*, 8192−8205.
(57) Ma, L.; Wang, Y.; Liu, Y.; Zhang, S.; Chen, Y. Comparative study on prosthetic socket materials. *Comput. Model New Technol.* **2014**, *18*, 387−392.
(58) Al-Samed, H. A.; Al-maamori, M.; Hussein, A. A. The Effect of Reinforcement PolySilicon Rubber with Foam Liner on Tensile Set and Hardness. *J. Surv. Fish. Sci.* **2023**, *10* (1S), 5976−5986.
(59) Ickrath, P.; Wagner, M.; Scherzad, A.; Gehrke, T.; Burghartz, M.; Hagen, R.; Radeloff, K.; Kleinsasser, N.; Hackenberg, S. Time-Dependent Toxic and Genotoxic Effects of Zinc Oxide Nanoparticles after Long-Term and Repetitive Exposure to Human Mesenchymal Stem Cells. *Int. J. Environ. Res. Public Health* **2017**, *14* (12), No. 1590.
(60) Ng, C. T.; Yong, L. Q.; Hande, M. P.; Ong, C. N.; Yu, L. E.; Bay, B. H.; Baeg, G. H. Zinc oxide nanoparticles exhibit cytotoxicity and genotoxicity through oxidative stress responses in human lung fibroblasts and Drosophila melanogaster. *Int. J. Nanomed.* **2017**, *12*, 1621−1637.
(61) Hong, L.; Zhou, N. Advancements in zinc oxide nanofibers for enhanced rehabilitation and injury recovery: mechanisms, applications, and future directions. *J. Biol. Eng.* **2025**, *19* (1), No. 93.
(62) Xiao, D.; Huang, Y.; Fang, Z.; Liu, D.; Wang, Q.; Xu, Y.; Li, P.; Li, J. Zinc oxide nanoparticles for skin wound healing: A systematic review from the perspective of disease types. *Mater. Today Bio* **2025**, *34*, No. 102221.
(63) Chong, W. J.; Shen, S.; Li, Y.; Trinchi, A.; Pejak Simunec, D.; Kyratzis, I.; Sola, A.; Wen, C. Biodegradable PLA-ZnO nanocomposite biomaterials with antibacterial properties, tissue engineering viability, and enhanced biocompatibility. *Smart Mater. Manuf.* **2023**, *1*, No. 100004.
(64) Cierech, M.; Wojnarowicz, J.; Kolenda, A.; Krawczyk-Balska, A.; Prochwicz, E.; Woźniak, B.; Łojkowski, W.; Mierzwińska-Nastalska, E. Zinc Oxide Nanoparticles Cytotoxicity and Release from Newly Formed PMMA-ZnO Nanocomposites Designed for Denture Bases. *Nanomaterials* **2019**, *9* (9), No. 1318.

https://doi.org/10.1021/acsomega.5c09735
ACS Omega 2026, 11, 36528−36538